

ELECTROCHEMICAL MICROMACHINING AND PARAMETER OPTIMIZATION ON AZ31 ALLOY—ANN AND TOPSIS TECHNIQUES

N. Sivashankar^{1*}, R. Thanigaivelan² and K.G. Saravanan³

¹Department of Mechanical Engineering, Kongunadu College of Engineering and Technology (Autonomous), Trichy, Tamilnadu, India

²Department of Mechanical Engineering, A.K.T. Memorial College of Engineering and Technology, Kallakurichi, Tamilnadu, India

³Department of Mechanical Engineering, Sona College of Technology, Salem, Tamilnadu, India

(Received November 21, 2022; Revised March 24, 2023; Accepted May 18, 2023)

ABSTRACT. Electrochemical micromachining (ECM) is a nontraditional method used for machining operations in hard and light materials with fixed or varying parameters. In this study, magnesium AZ31 alloy was micro machined using two types of electrolyte supply systems, namely electrolyte flooding and minimum quantity electrolyte (MQE). Experimental investigations were performed using TOPSIS and artificial neural network (ANN) techniques with types of electrolyte supply system, electrolyte concentration (EC), duty cycle (%), and machining voltage (V) as the input parameters, and material removal rate (MRR) and over cut (OC) as the outputs. Single and multi-objective parameter optimization was performed using Taguchi, TOPSIS, and ANN techniques. The machined microholes were analyzed using scanning electron microscopy. According to the TOPSIS results, under optimal conditions, a high MRR value and minimum OC of 1.282 $\mu\text{m/s}$ and 66 μm , respectively, were obtained. The results of TOPSIS were verified using the developed ANN architecture.

KEY WORDS: Magnesium, AZ31 alloy, Electrochemical micromachining, Optimization, TOPSIS, ANN

INTRODUCTION

Magnesium alloy exhibit several properties, such as high strength, high machinability, lightness, and good damping, which make them suitable for industrial applications, such as automobiles, biomedicine, and aerospace [1]. Magnesium alloys are mainly used for weight reduction in vehicles, bio implants, and aero parts. They have also been widely preferred in clinical applications recently because of their biocompatibility [2]. However, rapid corrosion of magnesium and alloys thereof considerably limits their widespread applications [3]. Several contemporary studies have attempted to enhance the machinability, corrosion rate, material formability, and other properties of magnesium alloys. Ayhan *et al.* [4] investigated the influence of machining parameters for AZ91 micromachining; the minimum surface roughness during micro milling was obtained at a high cutter speed of 11,000 rpm, feed rate of 170 mm/min, and cut depth of 0.3 mm. An *et al.* [5] observed the influence of various parameters on a thin-walled cylindrical specimen of AZ31 Mg alloy by using multistage forming techniques. Process parameters had the most significant influence on parts with uniform thickness, and the optimal parameters for forming AZ31 were the forming temperature of 250 °C, feed rate of 250 mm/min, and a 10 mm diameter form tool.

Mg alloys are suitable alternatives for contemporary popular metals such as aluminum and titanium. Because of limitations such as poor corrosion and wear resistance ability, research on Mg corrosion is highly warranted [6]. Khaled *et al.* [7] studied the electrochemical behavior (ECB) of Mg AZ31 with a 0.5 M KOH solution; a rupture surface was formed, dissolved Mg ions were redeposited in the electrolyte, and a platelet surface was produced on the specimen. This was

*Corresponding author. E-mail: sivashankar1911@gmail.com

This work is licensed under the Creative Commons Attribution 4.0 International License

attributed to the internal stress in the system and passive film. Fatimah *et al.* [8] developed an anti-corrosive coating for Mg AZ31 alloy using the plasma electrolytic oxidation method and achieved a defects-free coating with 27.1% less porosity at electrolyte temperature of 298 K. Zhang *et al.* [9] investigated the influence of ionic liquids on Mg AZ31; immersion of AZ31 in ionic liquids led to the formation mud cracks and galvanic corrosion on the protective layer. Long immersion time led to increased interaction, leading to the formation of mud cracks. Oktay *et al.* [10] found that the corrosion behavior of Mg sheets developed by roll strip casting was significantly impacted by the microstructures of the as-obtained sheets. Ion sizes and intermetallic structures also influence the rate of corrosion in Mg alloys. Mg AZ31 alloy is prone to corrosion pits in a highly alkaline environment [11].

Although several studies have investigated corrosion prevention in AZ31 Mg alloys, optimization of machining parameters is also essential [12]. Sreenivasulu *et al.* [13] optimized the drilling parameters for Al-Mg-Si using the Taguchi and grey relational analysis method; the suggested optimal parameters for making the perfect drill were the spindle speed, feed rate, drill diameter, and point angle of 695 rpm, 26 mm/min, 10 mm, and 100°, respectively. For Mg AM60 alloy, optimal parameters for milling were determined by Sathyamoorthy *et al.* [14]. Under the optimum condition, the surface roughness (Ra) improved; feed rate was identified as the most dominant factor influencing surface roughness (76.18%), followed by cut depth and speed. Abhijith *et al.* [15] adopted the ABC algorithm technique to optimize the machining parameters for AZ31 alloy; improved Ra of 0.34995 μm was obtained at the cutting speed, tooth feed, and cut depth of 500 mm/min, 0.4 mm, and 0.374 mm, respectively. Lubricant use during machining considerably influences Ra improvement [16]. Junzhan *et al.* [17] found that when AZ91D is dry milled over AM50A at 6000 rpm, it is inflammable when a spark is provided. Liwei *et al.* [18] investigated the effect of high-speed cutting of AZ31 and found that it decreased the roughness of AZ31. In addition to traditional machining, nontraditional machining methods, such as electron beam machining, electrochemical micromachining (ECM), and ultrasonic machining, have also been used for producing micro parts [19]. Thanigaivelan *et al.* [20] investigated the influence of different tool electrodes and the shapes of electrode tips on ECM in stainless steel and found that the machining rate and overcut (OC) were influenced by the shape of the tool electrode tip. A sharp edge on the electrode induced high OC during machining because of high stray current. Soundarajan *et al.* [21] investigated the effect of tool coating on ECM with EC of 23 g/L, machining voltage of 15 V, and duty cycle of 85%. Ceramic-coated tools with OC of 31 μm performed better (43.1%) than a non-coated tool. Thanigaivelan *et al.* [22] optimized the drilling parameters for machining micro holes by using ECM on copper alloys and identified that the optimal parameters for drilling micro holes with the minimum OC were EC of 25 g/L, 9 V machining voltage, and frequency of 40 Hz.

Several studies have focused on conventional machinability and corrosion improvement for AZ31; however, fewer studies have investigated the influence of ECM for AZ31 as well as the behavior of AZ31 alloy attributes for a wide range of applications [23]. In this study, the experiments were planned based on the L_{18} orthogonal array (OA), single objective optimization was performed using the Taguchi method, and multi-objective optimization was performed using TOPSIS and ANN and their results were compared. Type of electrolyte supply was considered as one of the factors, and its effect on MRR and OC was evaluated.

EXPERIMENTAL

The ECM setup comprised a control unit, tool holder, and sump. The control unit was used to maintain the machining voltage, duty cycle, and pulse frequency of the fabrication machine setup, and a stepper motor was used to control the tool movement. An electrolyte supply system was attached separately with a filter arrangement. The ECM setup is depicted in Figure 1a. During the experiments, AZ31 with material composition of 3.1 wt.% Al, 0.73 wt.% Zn, 0.25 wt.% Mn, 0.02

wt.% Si, 0.005 wt.% Fe, 0.0014 wt.% Ca, and balance Mg was used. Specimens with thickness of 2 mm were used for machining. A sharp-edged steel tool with a diameter of 600 μm was considered as the electrode. The strong galvanic corrosive nature of AZ31 makes sodium nitrate (NaNO_3) electrolyte as a suitable electrolyte for these experiments. An electrolyte solution of NaNO_3 , a neutral salt, was formed with distilled water with different concentrations. The experimental plan was framed with L_{18} OA with machining parameters such as type of electrolyte, machining voltage (V), duty cycle (%), and EC. During electrolyte flooding, AZ31 surface reacts with the electrolyte and induces galvanic corrosion leading to surface defects [24]. Hence a separate arrangement ie MQE supply system is made to supply the electrolyte in drops with the help of micro flow control valve. The ECM with the MQE supply system is depicted in Figure 1b. At minimum drop electrolyte machining, the electrolyte was supplied at 120 drops per minute. Droplets were supplied with self-gravity force and between the inter electrode gap (IEG). The MRR and the increased hole diameter, termed as OC, were considered as output parameters. The MRR was computed with the total time required to complete a hole, and OC was calculated using electrode diameter and hole diameter from the image taken with an optical microscope (BX41M-N22MB with CMOS camera type). 'CARL ZEISS' sigma with Gemini column type model of field emission microscopy was used for SEM analysis. The machining parameters and experimental results are presented in Tables 1 and 2, respectively.

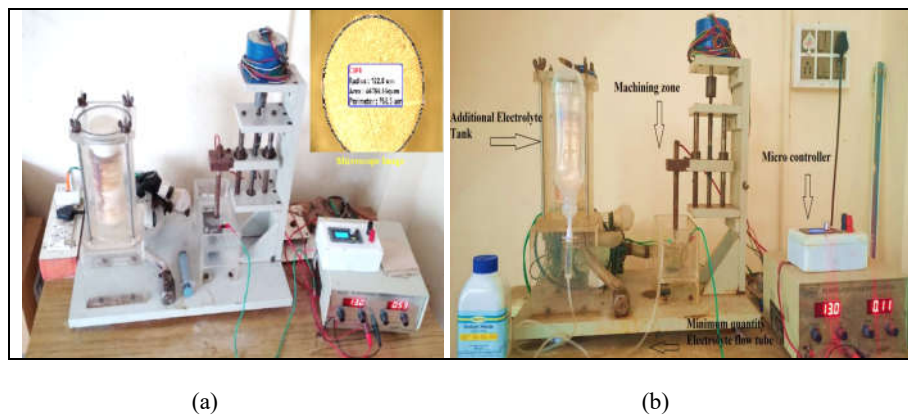


Figure 1. (a) ECM setup (electrolyte flooding type) and (b) modified ECM setup (MQE).

Table 1. ECM parameters and their levels.

Symbol	Control factors	Level 1	Level 2	Level 3
M	Type of electrolyte supply	Flooding of electrolyte	MQE	
V	Machining voltage (V)	9	11	13
D	Duty cycle (%)	50	62.5	75
E	Electrolyte concentration (g/L)	20	25	30

Table 2. ECM experimental results.

Sr. No	M	V	D	E	MRR ($\mu\text{m/s}$)	OC (μm)
1	1	9	50	20	0.317	57
2	1	9	62.5	25	0.358	64
3	1	9	75	30	0.556	88
4	1	11	50	20	0.407	52
5	1	11	62.5	25	0.521	67
6	1	11	75	30	0.617	76
7	1	13	50	25	1.075	92
8	1	13	62.5	30	1.282	66
9	1	13	75	20	0.980	121
10	2	9	50	30	0.278	79
11	2	9	62.5	20	0.282	63
12	2	9	75	25	0.444	70
13	2	11	50	25	0.330	59
14	2	11	62.5	30	0.362	51
15	2	11	75	20	0.427	62
16	2	13	50	30	0.595	102
17	2	13	62.5	20	0.606	94
18	2	13	75	25	0.513	126

RESULTS AND DISCUSSION

S/N ratio

The magnesium alloy AZ31 was machined with the input variables mentioned in Table 1, and the MRR and OC as output parameters were investigated. This study aimed to achieve high MRR with minimum OC. Computing the signal-to-noise (S/N) ratio (S/N) was the first step in mono-objective optimization, which was carried out using Minitab version 19. For high MRR, a higher value was considered to compute the response and lower value was better for OC. These are expressed in equations 1 and 2, respectively.

$$\text{MRR (Higher the better)} \longrightarrow \frac{S}{N} = -10 \log \left(\frac{\sum (\frac{1}{y^2})}{n} \right) \quad (1)$$

$$\text{OC (Smaller the better)} \longrightarrow S/N = -10 \log \frac{1}{n} \left(\sum_{i=1}^n y_i^2 \right) \quad (2)$$

where “n” denotes the experiments conducted and “y” denotes the data.

Figure 2a shows the mean effects plots for MRR drawn based on analyses. $M_1V_3D_3E_3$ were determined to be suitable parameters for achieving high MRR. In flooded electrolyte condition, the tool as well as the work piece was submerged into the electrolyte, which facilitated electron ion flow through the electrolyte. Machined debris was deposited near the machining zone, and it conducted more stray current, which increased the MRR in the submerged state [21]. Optimal machining parameters for MRR were determined to be 13 V, 75% D, and 30 g/L EC. High interactions between stray current and the AZ31 alloy increased the MRR. These results are in agreement with those of Maniraj *et al.* [19]. Analysis of variance analysis (ANOVA) was conducted with respect to MRR to determine the contribution of each parameter. The results showed that machining voltage most significant influenced MRR (55.78%), followed by type of electrolyte supply (20.92%). Further, minimum contribution of duty cycle and EC was observed. This was because of a direct interaction between the AZ31 alloy and stray current during electrolyte flooding.

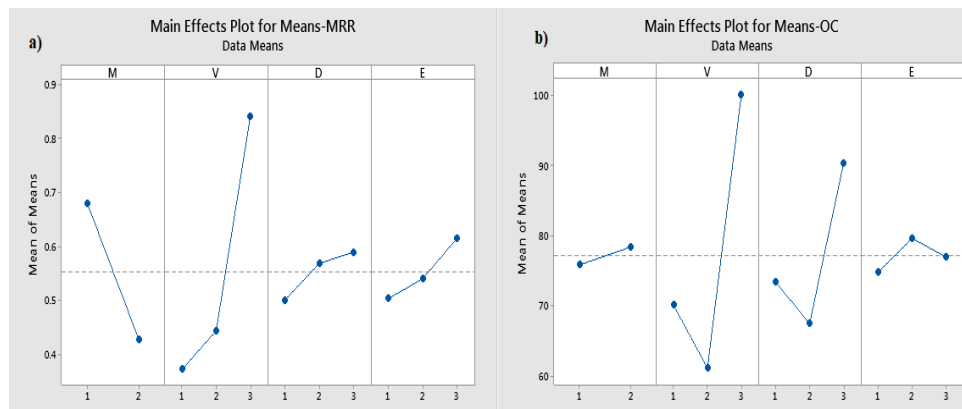


Figure 2. Mean effects of a) plot-MRR and b) plot-OC.

The mean effects plot in Figure 2b reveals the significant findings. In the MQE method, the electrolyte was supplied drop by drop between the IEG and work piece. Due to this the development of hydrogen bubbles was slowed down and interruption of machining is reduced. This mechanism decreased the stray current effect as well as the OC. Based on ANOVA, machining voltage (V) contributes higher percentage, i.e. 58.96%, followed by duty cycle (20.13%). Higher voltage and duty cycle led to higher OC because of the formation of micro sparks between IEG [20]. Figure 2b clearly shows that $M_2V_3D_3E_2$ were the optimum parameters for machining micro holes in the AZ31 alloy with minimum OC.

TOPSIS optimization

TOPSIS method of optimization is used to determine the suitable parameters in a multi-objective manner. It considers all parameters as inputs for determining the optimal solution. Herein, a decision matrix was considered as the beginning step, as presented in Equation 3. Thereafter, weights were allocated for each response. Finally, normalized values were calculated, as expressed in Equation 4, by considering the decision matrix and equal weightage.

$$r_{ij} = \frac{a_{ij}}{\sqrt{\sum_{i=1}^m a_{ij}^2}} \longrightarrow (3)$$

$$V_{ij} = W_i \times r_{ij} \longrightarrow (4)$$

Next, separation measures in the ideal solution, represented by S^+ and S^- , are given in equations 5 and 6, respectively

$$S_i^+ = \sqrt{\sum_{j=1}^M (v_{ij} - v_j^+)^2} \longrightarrow (5)$$

$$S_i^- = \sqrt{\sum_{j=1}^M (v_{ij} - v_j^-)^2} \longrightarrow (6)$$

Finally, the closeness coefficient (CC) was calculated to allocate the rank of each experiment, as given in Equation

$$CC_i = \frac{S_i^-}{S_i^+ + S_i^-} \longrightarrow (7)$$

Table 3 presents the TOPSIS multi-parameter optimization results, including normalization, weightage, and CC. Both MRR and OC were considered equally for the calculation of normalized weightage.

Table 3. Normalized, separation measures, and CC values.

Exp. no	Normalization		Weighted normalized		Separation measures		CC*
	MRR	OC	MRR	OC	S+	S-	
1	0.1209	0.1676	0.0604	0.0838	0.18422	0.10171	0.356
2	0.1365	0.1882	0.0683	0.0941	0.17722	0.09242	0.343
3	0.2120	0.2587	0.1060	0.1294	0.14874	0.07701	0.341
4	0.1552	0.1529	0.0776	0.0764	0.16685	0.11154	0.401
5	0.1987	0.1970	0.0993	0.0985	0.14700	0.09834	0.401
6	0.2353	0.2235	0.1177	0.1117	0.13202	0.09789	0.426
7	0.4100	0.2705	0.2050	0.1353	0.07205	0.15998	0.689
8	0.4889	0.1941	0.2445	0.0970	0.02205	0.21079	0.905
9	0.3737	0.3558	0.1869	0.1779	0.11793	0.13406	0.532
10	0.1060	0.2323	0.0530	0.1161	0.19582	0.06910	0.261
11	0.1075	0.1852	0.0538	0.0926	0.19150	0.09262	0.326
12	0.1693	0.2058	0.0847	0.1029	0.16221	0.08820	0.352
13	0.1259	0.1735	0.0629	0.0867	0.18191	0.09900	0.352
14	0.1381	0.1500	0.0690	0.0750	0.17543	0.11142	0.388
15	0.1628	0.1823	0.0814	0.0911	0.16383	0.09828	0.375
16	0.2269	0.2999	0.1135	0.1500	0.15094	0.06999	0.317
17	0.2311	0.2764	0.1156	0.1382	0.14357	0.07826	0.353
18	0.1956	0.3705	0.0978	0.1852	0.18346	0.04481	0.196

As shown in Table 3, maximum CC value (0.905) was obtained in experiment 8. Based on the computed CC value, ranks were assigned to each experiment. Based on CC-based rank, experiment run order was $8 > 7 > 9 > 6 > 4 > 5 > 14 > 15 > 1 > 17 > 12 > 13 > 2 > 3 > 11 > 16 > 10 > 18$. Based on the CC value, responses were calculated (Table 4), and machining voltage (V) was determined to be highly dominant, followed by machining method and other parameters. These findings are similar to those of single objective optimization (Figure 2). As shown in Figure 3, 13 V flooded electrolyte, 62.5% duty cycle, and 30 g/L EC were the optimal parameters for drilling micro holes in AZ31 alloy specimen with high MRR and minimum OC. At the maximum voltage, high current density in the IEG induced the high MRR. Due to the change in duty cycle, flow of electrons resist the spark production between IEG was reduced and directly impacted on OC. ANOVA was performed for TOPSIS, and the results are presented in Table 5.

Table 4. Response table for means-CC*.

Level	M	V	D	E
1	0.4882	0.3298	0.3960	0.3904
2	0.3245	0.3905	0.4527	0.3890
3	-	0.4988	0.3704	0.4397
Delta	0.1637	0.1690	0.0823	0.0507
Rank	2	1	3	4

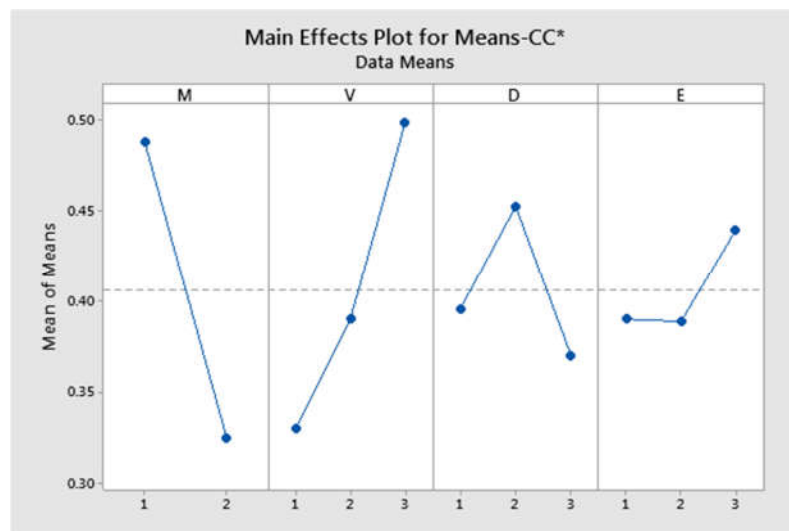


Figure 3. Mean effects plot-CC*.

Table 5 Analysis of variance-CC*.

Source	DF	Adj SS	Adj MS	F-value	P-value	%
M	1	0.12052	0.120519	5.84	0.036	27.02
V	2	0.08795	0.043976	2.13	0.169	19.72
D	2	0.02128	0.010639	0.52	0.612	4.77
E	2	0.01002	0.005009	0.24	0.789	2.25
Error	10	0.20622	0.020622	-	-	46.24
Total	17	0.44599	-	-	-	100.00

Findings of ANOVA showed that type of electrolyte supply plays a crucial role in machining micro holes in AZ31 alloy specimens (contribution rate = 27.02%), followed by machining voltage (19.72%). These results are similar to the findings of mono-objective optimization. Both D and E showed minimum effect on MRR and OC. The contribution rate of duty cycle on the MRR and OC was only 4.77%, followed by EC (2.25%).

ANN optimization

ANN architecture was developed using MATLAB'15 to validate the TOPSIS results. In ANN, a 4 (10) 1 type of architecture generally provides highly accurate results for parameter optimization [25-28]. The developed ANN model was trained with same experimental results and included in MATLAB. To train the ANN model, training values, target, and test outputs were used. Totally 5000 iterations were required to obtain highly optimum results. The variables used for ANN training are presented in Figure 4a. The ANN model comprised two layers, namely hidden layer and output layer, as shown in Figure 4a.

Based on the training, the regression curve was plotted (Figure 4b). Clearly, the developed model produced an R value of 95.27% during training. In the developed model, the overall R value was 96.2%. Validation was performed with an R value of 99.98%. Overall, the developed

ANN model produced highly accurate test results. Hence, TOPSIS prediction results and optimization values were used as test values in the trained ANN model. It could accurately predict the MRR value as $1.27 \mu\text{m/s}$, which was very close to the TOPSIS optimized value of $1.282 \mu\text{m/s}$, and OC was predicted to be $51 \mu\text{m}$, which is similar to the initial process parameters. Confirmation experiments were performed with the obtained optimal parameters. Based on consideration of the multi-input parameters, $M_1V_3D_2E_3$ were identified as the optimal parameters with MRR value of $1.282 \mu\text{m/s}$ and minimum OC of $66 \mu\text{m}$. CC was found to improve by 54.9%, and micro holes were made in the AZ31 alloy specimen with optimum parameters of 13 V, 62.5% duty cycle, and 30 g/L EC. Scanning electron microscopy (SEM- CARL ZEISS' sigma type) was performed on the machined material to observe surface quality and hole geometry. SEM images of AZ31 are presented in Figure 5a.

The surface of the machined micro hole on AZ31 was affected by galvanic corrosion, which led to the formation of pits and delaminated edges. NaNO_3 reacted with the AZ31 alloy and produced magnesium oxide. Stray current affected the surface of the AZ31 alloy and produced a white layer along the circumference of the machined hole. A magnified image of the circumference of the machined hole is presented in Figure 5b. Delaminated edges and pits were formed on the hole boundaries due to electrolyte flooding machining. In the submerged state, the electrolyte reacted with the surface of the AZ31 alloy and resulted in galvanic corrosion. While machining, debris was collected, and SEM analysis was performed at $100 \mu\text{m}$ scale, as presented in Figure 5c. Crystal grains such as debris were observed in the solid state, thus demonstrating high-quality machining.

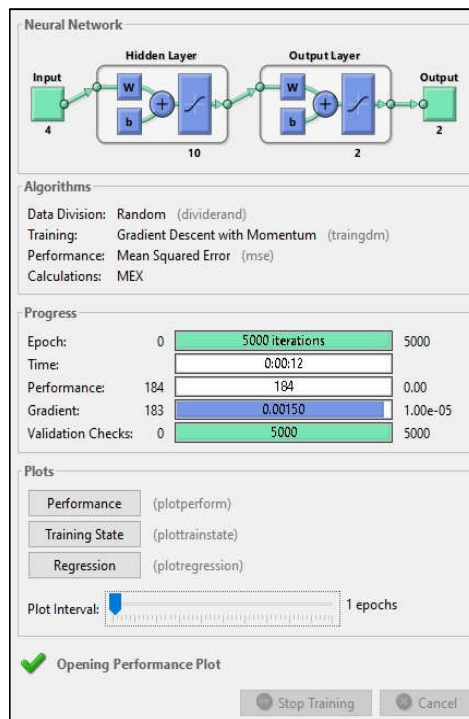


Figure 4 a) ANN architecture.

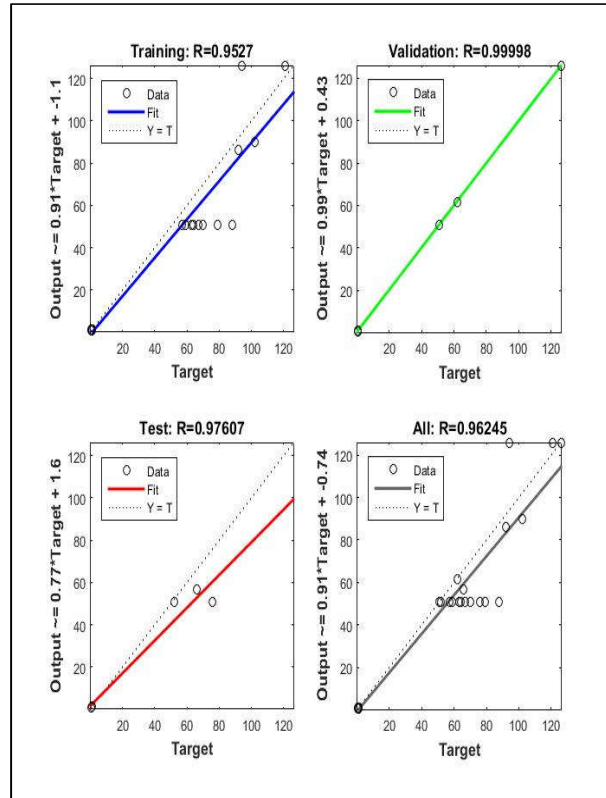


Figure 4 b) Regression curves.

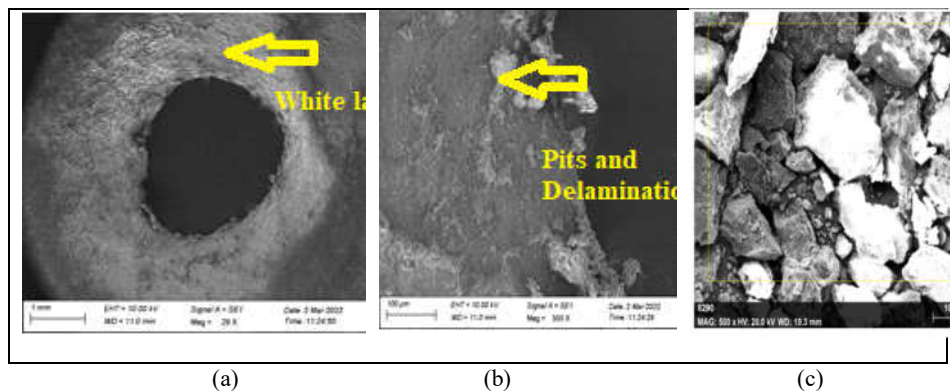


Figure 5. a) Micro hole in AZ31 under optimum conditions, b) surface of AZ31 with defects, and c) AZ31 machined debris.

CONCLUSION

AZ31 alloy was used in ECM using electrolyte flooding and MQE conditions, and the operating parameters were optimized. The findings of this study are as follows: (1) In single-parameter optimization, i.e., electrolyte flooding machining, $M_1V_3D_3E_3$ were identified as suitable parameters for achieving high MRR, with 13 V machining voltage, 75% duty cycle, and 30 g/L EC. (2) For minimum OC, i.e., MQE machining, $M_2V_3D_3E_2$ were the optimal parameters, with 13 V machining voltage, 75% duty cycle, and 25 g/L EC. (3) The proposed MQE machining method directly influences the process by reducing OC and resulting in fewer defects. (4) Based on TOPSIS, for electrolyte flooding machining, 13 V, 62.5 duty cycle, and 30 g/L EC ($M_1V_3D_2E_3$) were identified as the optimal parameters, which yielded the MRR value of 1.282 $\mu\text{m/s}$ and minimum OC of 66 μm . (5) SEM analysis revealed that galvanic corrosion influenced the surface of hole boundary and delaminated edges. (6) An ANN model with 4 (10) 1 type of architecture was developed and trained with 5000 iterations to compare the TOPSIS predictions. Based on ANN prediction, MRR value of 1.27 $\mu\text{m/s}$ and OC value of 51 μm were deemed suitable for $M_1V_3D_2E_3$. (7) This study explored the influence of MQE machining and parameter optimization in AZ31 alloy with NaNO_3 electrolyte.

REFERENCES

- Jahangir, Md.; Mamun, M.A.H.; Michael, P.S. A review of additive manufacturing of magnesium alloys. *AIP Conference Proceedings*. **2018**, 1980, 030026.
- Zong, Y.; Yuan, G.; Zhang, X.; Mao, L.; Niu, J.; Ding, W. Comparison of biodegradable behaviors of AZ31 and Mg–Nd–Zn–Zr alloys in Hank's physiological solution. *Mater. Sci. Eng. B* **2012**, 177, 395-401.
- Tan, J.; Ramakrishna, S. Applications of magnesium and its alloys: A review. *Appl. Sci.* **2021**, 11, 6861.
- Ayhan, E.; Umut, A. Investigation of the effects of machining parameters on surface integrity in micromachining. *Open Chem.* **2022**, 20, 212-224.
- An, Z.; Yan, D.; Qie, J.; Lu, Z.; Gao, Z. Effect of process parameters on formability of a AZ31 magnesium alloy thin-walled cylindrical part formed by multistage warm single-point incremental forming. *Front. Mater.* **2020**, 7, 151.
- Rakshith, M.; Seenuvasaperumal, P. Review on the effect of different processing techniques on the microstructure and mechanical behaviour of AZ31 magnesium alloy. *J. Magnes. Alloy.* **2021**, 9, 1692-1714.
- Khaled, M.I.; Sannakaisa, V. Electrochemical behavior of magnesium alloy AZ31 in 0.5 M KOH solution. *Electrochem. Solid-State Lett.* 2007, 10, 3.
- Fatimah, S.; Kamil, M.P.; Han, D.I.; Al-Zoubi, W.; Ko, Y.G. Development of anti-corrosive coating on AZ31 Mg alloy subjected to plasma electrolytic oxidation at sub-zero temperature. *J. Magnes. Alloy* **2022** 10, 7, 1915-1929.
- Zhang, Y.F.; Hinton, B.; Wallace, G.; Liu, X.; Forsyth, M. On corrosion behaviour of magnesium alloy AZ31 in simulated body fluids and influence of ionic liquid pretreatments. *Corros. Eng. Sci. Technol.* **2012**, 47, 374-382.
- Oktay, G.; Ürgen, M. Corrosion behaviour of magnesium AZ31 sheet produced by twin roll casting. *Corros. Eng. Sci. Technol.* **2015**, 50, 380-389.
- Doja, S.; Bichler, B.; Fan, S. Corrosion behavior of AZ31 magnesium alloy in highly alkaline environment. *Acta Metall. Sin. (Engl. Lett.)* **2017**, 30, 367-375.
- Muthuram, N.; Christo Frank, F. Optimization of machining parameters using artificial Intelligence techniques. *Mater. Today: Proc.* **2021**, 46, 8097-8102.
- Sreenivasulu, R.; Srinivasarao, C. Optimization of drilling parameters during machining of al-mg-si alloys by taguchi method coupled with grey relational analysis and validated by Fea based deform – 3D. *J. Mech. Eng.* **2021**, 71, 221-238.

14. Sathyamoorthy, V.; Deepan, S.; SathyaPrasanth, S. P.; Prabhu, L. Optimization of machining parameters for surface roughness in end milling of magnesium AM60 alloy. *Indian J. Sci. Technol.* **2017**, *10*, 1-7.
15. Abhijith; Srinivasa, P.; D'Mello, G.; Hebbar, G. Surface roughness optimization in machining of AZ31 magnesium alloy using ABC algorithm. *MATEC Web. Conf.* **2018**, *144*, 03006.
16. Ibrahim, G.A.; Burhanuddin, Y.; Emrijakto, D. A study on drill machining for magnesium alloy using Taguchi method. *IOP Conf. Series: Mater. Sci. Eng.* **2020**, *857*, 012014.
17. Hou, J.Z.; Wei, Z.; Zhao, N. Effect of cutting parameters on ignition of AM50A Mg alloy during face milling. *Mater. Manuf. Process.* **2010**, *25*, 1048-1051.
18. Liwei, L.; Shaohua, H.; Longfei, L.; Zhenru, Y. High speed cutting of AZ31 magnesium alloy. *J. Magnes. Alloy.* **2016**, *4*, 128-134.
19. Maniraj, S.; Thanigaivelan, R. Optimization of electrochemical micromachining process parameters for machining of AMCs with different % compositions of GGBS using Taguchi and TOPSIS methods. *Trans. Indian Inst. Met.* **2019**, *72*, 3057-3066.
20. Thanigaivelan, R.; Arunachalam, R.M. Experimental study on the influence of tool electrode tip shape on electrochemical micromachining of 304 stainless steel. *Mater. Manuf. Process.* **2010**, *25*, 1181-1185.
21. Soundarrajan, M.; Thanigaivelan, R. Effect of coated and geometrically modified tools on performance of electrochemical micromachining. *Mater. Manuf. Process.* **2020**, *35*, 775-782.
22. Thanigaivelan, R.; Arunachalam, R.M.; Pelden Drukpa. Drilling of micro-holes on copper using electrochemical micromachining. *Int. J. Adv. Manuf. Technol.* **2012**, *61*, 1185-1190.
23. Ramesh, S.; Viswanathan, R.; Ambika, S. Measurement and optimization of surface roughness and tool wear via grey relational analysis TOPSIS and RSA techniques. *Measurement*, **2015**, *78*, 63-72.
24. Lee, E.S.; Won, J.K.; Shin, T.H.; Kim, S.H. Investigation of machining characteristics for electrochemical micro-deburring of the AZ31 lightweight magnesium alloy. *Int. J. Precis. Eng.* **2012**, *13*, 3, 339-345.
25. Kosarac, A.; Mladjenovic, C.; Zeljkovic, M.; Tabakovic, S.; Knezev, M. Neural-network-based approaches for optimization of machining parameters using small dataset. *Materials* **2022**, *15*, 700.
26. Doriana, M.; D'Addona; Teti, R. Genetic algorithm-based optimization of cutting parameters in turning processes. *Procedia CIRP* **2013**, *7*, 323-328.
27. Sangwan, K.S.; Saxena, S.; Kant, G. Optimization of machining parameters to minimize surface roughness using integrated ANN-GA approach. *Procedia CIRP* **2015**, *29*, 305-310.
28. Nalajam, P.; Varadarajan, R. Experimental and theoretical investigations on cold metal transfer welds using neural networks: A computational model of weld geometry. *Exp. Tech.* **2021**, *45*, 705-720.